Effect of spherical dents on microstructure evolution and rolling contact fatigue of wheel/rail materials

Effect of spherical dents on microstructure evolution and rolling contact fatigue of wheel/rail materials

X.J. Zhao[1, 2], J.Guo[1], Q.Y. Liu[1], E. Butini[2], L. Marini[2], E. Meli[2], A. Rindi[2], W.J. Wang[1,*]

1. Tribology Research Institute, State Key Laboratory of Traction Power, Southwest Jiaotong University, Chengdu 610031 2. Department of Industrial Engineering, University of Florence, Via S. Marta 3, 50139 Firenze, Italy

Abstract: Surface dents may occur on both rail head and wheel tread and have a deep influence on their microstructures. This investigation aims at exploring the microstructure evolution and RCF of wheel/rail materials with spherical dents. The experimental results, obtained through a suitable instrumented roller-rig, highlight the different microstructure evolutions not only between rail and wheel, but also between front and rear areas of dent. Electron backscattered diffraction data shows that the grains around dent on wheel have higher strain, misorientation and quantity of large angle grain boundaries than those on rail roller, leading to a weaker RCF resistance in wheel rollers. Meanwhile, cracks tend to propagate in front area of dent on rail and rear area of dent on wheel.

Keywords: Wheel/rail materials; Spherical dents; RCF; Microstructure evolution

1. Introduction

The rolling contact fatigue caused by cyclic rolling contact between the wheel tread and rail head, has significant effects on service life of wheel/rail materials. Initial researches demonstrated how factors such as rolling direction [1], contact pressure distribution [2], and fluid entrapment [3] affects the RCF of wheel/rail materials. Furthermore, to meet the increasing demand for speed and load capacity coming from modern railway transportation,

*Corresponding author. Tel: +86-28-87634304.

E-mail address: wwj527@swjtu.cn (W.J. Wang).

https://doi.org/10.1016/j.triboint.2018.07.001

the high-speed and heavy-haul railway systems have rapidly developed, leading to new damage types potentially connected to RCF. Nowadays, there is a number of different failures that appear on wheel/rail surface such as corrugation [4], squats [5], head checks [6] and wheel flat [7].

With the progress of sensors on test machines and of computer hardware, many studies have been carried out to explore the wear behaviors and wheel/rail RCF life by means of various experimental and numerical methods. Zhu [8] pointed out that, either increasing surface roughness or having thick oxides increases wear, while, thin oxides help to protect contacting surfaces, producing negligible wear and a smooth surface. Compared with the experimental result, Daves [9] set a multi-scale model and predicted the crack growth direction considering stick-slip behaviour of wheel/rail contact. By changing the attack angle on wheel rail surface, Huang [10] found that RCF cracks tend to grow in depth on the rail rollers while they are easy to become parallel to the surface on the wheel rollers. Ekberg [11] showed how stress gradient (especially in highly stressed regions) should be dealt with in fatigue design analyses. Ignesti [12] and Innocenti [13] established a development model for wheel and rail profile to predict their service lives. Nejad [14] pointed out that the fatigue life decreases with an increase of the stress field in wheel-rail contact zone. By means of numerical method, Taraf [15] found that defects or small friction coefficient are a plausible explanation to the initiation of deep subsurface fatigue cracks.

The surface damage could be another inducement for RCF cracks initiation. The surface damage can be caused by the hard body coming from the external environment. The hard body may stem from the drop of freight train goods (such as the minerals), or the ballast

stones rolled up by the passage of the trains. Once the hard body entered the wheel/rail interface and crashed, the damage occurs both on the rail and wheel surfaces. Subsequently, in the service phase, this surface damage will change the contact condition and affect the service life. Therefore, a large number of researches have been carried out to study the effect of surface damage on wheel/rail materials in recent years. Using full scale experimental method, Stefano [16] detected the vertical RCF cracks around the dents on the wheel tread. Based on evolution process of different dent shapes on rail surface, Gao [17-18] found that conical and pyramidal dents had an obvious influence on fatigue life while neither transverse nor longitudinal scratches had any influence on disc life. Seo [19] pointed out that the RCF cracks would initiate and propagate when the diameter of dents reaches a certain size.

In this study, the role played by surface spherical dents in the microstructure evolution and wheel/rail RCF is carefully investigated. The experiments for investigating the effects of spherical dents on RCF of wheel/rail materials were performed by using a rolling-sliding wear testing machine. In particular, the microstructure evolution of wheel/rail materials around the dents was also exhibited through Electron Backscattered Diffraction (EBSD) measures. The relationship between microstructure of wheel/rail material and RCF cracks around the dents were discussed. The experimental results highlight the different microstructure evolutions not only between rail and wheel materials, but also between front and rear areas of the dent. More particularly, EBSD data shows that the grains around the dent on wheel roller have higher strain, misorientation and quantity of large angle grain boundaries than those on rail roller, leading to a weaker RCF resistance in wheel rollers. Meanwhile, cracks tend to propagate in the front area of dent on rail roller and the rear area of dent on wheel roller.

2. Experimental details

2.1 Experimental machine

All experiments were carried out using a rolling-sliding wear testing machine composed of a wheel specimen (lower roller) and a rail specimen (upper roller) [20]. Two rollers are powered and controlled by a DC motor (Fig.1). The transmission gears transmit the power from drive shaft to driven shaft. The slippage between the wheel/rail rollers can be altered by changing the transmission gear pairs. The upper specimen is fixed in a swinging bracket where a normal force (from 0 to 2000 N) can be applied and adjusted by a compressed spring; the normal force is measured by a force sensor. The tangential and normal forces in the wheel/rail interface are automatically measured by means of the torque sensor (3) and load sensor (11) (measurement error: ±5%); the instant friction coefficient can be calculate based on the signals captured by these sensors.

2.2 Experimental parameters

The wheel and rail rollers were cut from the wheel tread and rail head, respectively. The scheme size of wheel and rail rollers are shown in Fig.2. Their chemical compositions in weight percentage are given in Table 1. The normal force of 347 N is applied on the wheel/rail interface. The slippage is 0.91% and rotational speed of wheel roller is 200 r/min (about 0.42 m/s). Referring to the shape of dent mentioned in UIC standard 712R [21] and the size of dent on rail roller in previous paper [19], the diameters of dents on rail rollers are 1.1, 1.5 and 1.8mm, respectively, which are impacted by a pendulum machine (a steel ball from bearing with diameter of 3 mm is fixed on the hammer) with the impact energy of 12 000, 15 000 and 17 000 J, respectively. Then, the dents on wheel rollers were impacted by the hammer with

the same impact energy. The nomenclature used hereinafter has the first letter related to the material (R for rail and W for wheel), followed by a letter related the size of dents (N for non-dent, S, M and L for small, middle and large). The profile of spherical dents is shown in Fig.3. The defected rail and wheel rollers are matched to non-defected wheel and rail rollers, respectively. The total cycles is set at 96 000, and, to consider actual operating conditions, the test is stopped every 12 000 cycles and wheel roller is reversed in the meantime. So, the rolling direction of wheel roller changes periodically, the ~~while~~ rail rollers always rotate at one direction and the slippage is kept constant. All experimental parameters are listed in Table 2.

In this study, all experiments were carried out under controlled environmental conditions (temperature: 20~23 ℃, relative humidity: 40~60%). The plastic deformation, surface damage and cracks were examined by optical microscope (OM) (OLYMPUS DSX510, Japan) and scanning electron microscope (SEM) (JSM-7001F, Japan). The grain boundary, grain misorientation and inversed pole figure (IPF) are obtained by Electron Backscattered Diffraction (EBSD). The test rollers were cut longitudinally along the rolling direction. After polishing the samples to a roughness equal to 0.5 μm, the samples were etched by ethanol with 4% HNO_3 for analyzing with SEM.

3. Results

3.1 Surface damage

SEM micrographs of surface damage on rail rollers are shown in Fig.4. It is obvious that the material accumulates on one side of the dents. Compared to the rail roller without dents,

the crest appears on the surface of defected rail rollers. Besides, with the size of dent increasing, the crest becomes more visible as well as the adhesion spots on it (Figs.4b-d). As for the surface cracks, it seems to alleviate when the small dents emerge on the rail roller (Figs.4a, b). However, the surface cracks aggravate with the size dents enlarging (Figs.4c, d).

The surface damage behavior changes on wheel rollers, as Fig.5 shows. The dents tend to be coved by accumulated material from different directions. There are seldom adhesion spots on the wheel roller, which may be due to the fact that wheel material has a lower hardness than rail material. Moreover, only plastic flow and small peelings appear on RN rollers while, on the defected rollers, the surface cracks dominate. In particular, some dark dots gathered around the dent (Fig.5c) are present; these dark dots might be the dislocation pile-up group. Because of the residual stress caused by the dent, dislocations begin to glide or climb and finally piled up at surface [22].

3.2 Plastic deformation and subsurface damage

Fig.6 shows a different plastic deformation extent of rail material around dent. Along the direction of tangential force, the sample profile can be divided into two areas by dent: front area and rear area. The depth of deformation in the front area is larger than that in the rear area. Due to the reverse of rolling direction, the deformation characteristics of wheel roller vary (Fig.7). Within certain scale near the dent, the front and rear areas have opposite direction of plastic deformation. It is noteworthy that the deformation depth on front area gradually declines and the deformed line finally changes into an opposite direction. As Fig.7 shows, the length of transition zone declines from 1054 to 713 μm as the dent increases from small to large.

Fig.8 shows the fatigue cracks on the section of rail rollers. The statistics about these cracks on rail rollers are listed in Table.3. As it shows, due to the different depth of plastic deformation near the dent, cracks seem easier to initiate in front area than in rear area. More importantly, the length of the crack in front area is 1.12 times that in rear area (RS roller), then this ratio further increases up to 1.78 times with size of dent rising (RL roller).

In order to reveal the relationship between deformation and tiny cracks, SEM micrographs with high magnification was applied on front and rear areas of dent. Compared to regular deformed line in Fig. 9a, the deformed line is distorted in the edge of dent. This may attribute to the cyclic impact when the dent entering wheel/rail interface. A small cyclic impact may densify the pearlite (Fig.9b) or could be an inducement for vertical crack initiation (Fig.9c). However, the crack would fracture due to the fact that the deformed line is distorted at a sharp angle by the increasing cyclic impact.

Since the tangential force on wheel roller reverses frequently, the deformation line and the crack propagation behavior changes at each period. In yellow square of Fig.10 (standing for “front area”), the deformed line rolls up the pearlite (Fig.10c) or even the cracks (Fig.10d), making the cracks propagating at unpredictable angles. In the blue square (standing for “rear area”), cracks initiate and grow in length. It can be concluded from Fig.10 that cracks in rear area is longer than that in front area. Table 4 compares the types of crack around dent in wheel and rail materials. The crack growth in depth can be detected in all the defected wheel samples while it can be only found in RM roller. Meanwhile, the branch cracks often emerge on the wheel rollers. Therefore, it can be inferred that the subsurface damage on defected wheel roller is as severe as that on rail roller.

3.3 Grain characteristics

The EBSD method is focused on the deformed grains on wheel and rail rollers with dent. Therefore, the test areas are selected at about 50 μm below the surface. Fig.11 reveals the distinct differences of grain angle between rail and wheel rollers. The black line sketches the grains boundary with large angle (more than 15 degree) while the green line stands for the grains boundary with small angle (from 2 up to 15 degree). It is obvious from Fig.11a that grains with large angle gather near the surface and become less frequent inside the body. However, the grains with large angle boundary dominate on defected wheel roller as Figs.11b-c show. On the contrary, the situation changes on the defected rail roller, especially in the rear of the dent. In this case, the majority of grains are characterized by small boundary angle. It can be attribute to the fact that the slight deformation in the rear area assures less energy to disorder the grains.

The inversed pole figure (IPF) shows the crystal orientation of each grain on rail and wheel rollers. The similar color presents a same orientation trend for grains. The gains orientation in wheel roller shows a clear anisotropy phenomenon (Fig.12b). Only a few fiber textures with small misorientation can be found in the rear of dent (Fig.12c). Conversely, the grains in rail roller share an almost similar crystal orientation, especially in rear of dent (Fig.12e).

The strain distribution on wheel and rail roller after testing is shown in Fig.13. On WN rollers, the high strain areas are concentrated near the surface at the maximum value of 9.55. When a dent appears on wheel roller, the strain increases immediately up to 16.55. On the contrary, the strain on rail roller shows an extremely low value at 5.85 and it decreases rapidly

towards the inside of the body. Finally, it has to be noticed that the average strain in rear area seems lower than that in front area, both in wheel and rail rollers.

4. Discussion

Adhesion describes the tangential force resulting at the wheel–rail contact [23]. In these ~~is~~ experiments, the slippage is set as 0.91%, which provides a relatively high adhesion coefficient between the rail/wheel surface [24]. This way, the tangential force acting on the contact area is large enough to drastically change the microstructure of grains and cause severe plastic deformation. Severe plastic deformation of the wheel/rail materials caused by the heavy and cyclic contact loading is known to have a great influence on RCF crack initiation [25]. The wear rate and material ratcheting are coupled factors which determine the depth of plastic deformation. Fig.14a shows material movement in front and rear areas on defected rail roller. In the edge of the front area, the tangential force compels the material sliding and forms an accumulation layer. As a result, the plastic deformation fills up the dent on one side. On the other hand, in the rear area, the tangential force can be divided into two components acting on the edge of dent. Since the edge of dent is not parallel to the surface, one of the force component rapidly removes material at the edge of dent and leaves a slope there. The second force component acts on this slope again and then the material is removed layer by layer. Therefore, the depth of plastic deformation in the front area is larger than that in the rear area as Fig. 6 presents. Due to such an unbalanced deformation distribution, the yield strain in the front area is more than 2 times the strain in the rear area. It can be inferred from Figs.12 and 13 that a high strain area is usually associated with large misorientation, and

a large misorientation facilitates the onset of small cracks [26]. The grain in the front area of dent has larger misorientation than that in rear area on rail roller (Fig. 14(b)). Thus, the cracks in front area on rail roller is more severe than that in rear area (as Table 3 shows).

Because of the inversion of tangential force on wheel roller, the “front area” in the previous period turns into “rear area” in the current period. As it is mentioned above, the rear area of the dent has a higher wear rate. In the primary cycles, the material accumulates in the front area of dent (Fig.15a). Subsequently, the plastic deformation is easily worn and forms a new plastic deformation layer with single flow direction as the “front area” changes into “rear area”. As a result, a fiber texture with small misorientation emerges in the rear of dent. As a previous paper mentions [26], tiny cracks tend to propagate in the area with small misorientation (Fig.15b). The other side of dent experiences the transformation from “rear area” into “front area”. Due to low wear rate in “front area”, the microstructure is affected by two plastic deformation lines with different flow directions. The previous plastic deformation is rolled up (Fig.6), the continuous fiber texture is destroyed (Fig.12b) and the microstructure is mainly anisotropic, which slows down the crack growth. This way, the crack in rear area of dent on wheel roller is longer than that in the front area (Fig.10).

The quantity of large angle grain boundary can be another index to estimate microstructure performance; in fact, large angle grain boundary means high lattice distortion energy, which is also related to yield strain. Considering the frequent tangential force inversion on wheel roller, each grain in the deformed area is compelled to shape in line under a direction-changing force. Thus, the quantity of large angle grain boundary in wheel roller is so large that high strains are present. However, the plastic deformation alleviates especially in

rear area of the dent on rail roller (there is a few quantity of large angle grain boundary and it even decreases rapidly in depth). Therefore, the strain in defected rail roller achieves an extremely low value and drops sharply towards the inside of the body. As EBSD data indicate, the strain in defected wheel roller is approximately 3-6 times that in defected rail roller (Fig.13). The previous papers pointed out that highly strained grain can act as a crack propagation path [27, 28]. As a result, the cracks in defected rail roller are small and hard to propagate in depth, while the crack in defected wheel roller is long and grows in various directions.

In summary, the plastically accumulated material plays an important role in the material structure evolution. The material in the front and rear areas around the dent shows a different RCF performance due to the distinct grain microstructures. Moreover, the defected wheel roller has an inferior RCF resistance because of the high strain caused by the tangential force inversion. Therefore, in order to avoid severe damage on wheel/rail system, it is essential to clear the dent as much as possible, especially on wheel tread. ~~Moreover~~At the same time, cracks tend to propagate in the front area of the dent on rail roller and the rear area of the dent on wheel roller. In addition, in the further works, more EBSD tests and analyses ~~would be applied~~will be performed to systematically study ~~on~~ the microstructures of different kinds of dents (in terms of sizes and shapes). ~~in the further works.~~

5. Conclusions

After the whole experimental campaign on the roller rig and the detailed analysis of the experimental data, the following main conclusions can be drawn:

1. The depth of plastic deformation on defected rail roller is unbalanced around the dent. The area firstly entering the contact interface along the rolling direction has a thicker plastic deformation than that on the other side.

2. The strain, misorientation of grains and quantity of large angle grain boundaries around the dent on wheel roller are larger than that on rail roller.

3. Due to the different microstructure evolution under tangential force, the crack grows easily in the front area of dent on rail roller, while it tends to propagate in the rear area of dent on wheel roller.

4. The defected wheel roller has an inferior RCF resistance, if compared to the rail roller, because of the higher strain. The cracks on wheel rollers may grow in various directions.

Acknowledgments

The work is supported by the National Natural Science Foundation of China (Nos. 51775455, 51575460), the Autonomous Research Project of State Key Laboratory (No. 2018TPL-T02) and Innovation Foundation of Southwest Jiaotong University (No. D-CX201708).

References

[1] Tyfour WR, Beynon JH. The effect of rolling direction reversal on fatigue crack morphology and propagation. Tribol Int 1994; 27: 273-82.

[2] Guagliano M, Paub M. Analysis of internal cracks in railway wheels under experimentally determined pressure distributions. Tribol Int 2007; 40: 1147-60.

[3] Fletcher DI, Hyde P, Kapoor A. Modelling and full-scale trials to investigate fluid pressurization of rolling contact fatigue cracks. Wear 2008; 265:1317-24.

[4] Jin XS, Wen ZF, Wang KY, et al. Effect of a scratch on curved rail on initiation and evolution of rail corrugation. Tribol Int 2004; 37: 398-94.

[5] Grassie SL, Fletcher DI, Gallardo Hernandez EA, et al. Studs: a squat-type defect in rails. Proc IMechE, Part F: J Rail Rapid Transit 2011; 266: 243-56.

[6] Sato Y. Design of rail head profiles with full use of grinding. Wear 1991; 144: 363-72.

[7] Sackfield A, Dini D, Hills DA. The contact problem for a wheel having a 'flat'. Wear 2006; 261: 1265-70.

[8] Zhu Y, Chen X, Wang .W, et al. A study on iron oxides and surface roughness in dry and wet wheel/rail contacts. Wear 2015; 328-339: 241-48.

[9] Daves W, Kubin W, Scheriau S, et al. A finite element model to simulate the physical mechanisms of wear and crack initiation in wheel/rail contact. Wear 2016; 366-367 78-83.

[10] Huang YB, Shi LB, Zhao XJ, et al. On the formation and damage mechanism of rolling contact fatigue surface cracks of wheel/rail under the dry condition. Wear 2018; 400-401: 62-73.

[11] Ekberg A, Kabo E, Lundén R, et al. Stress gradient effects in surface initiated rolling contact fatigue of rails and wheels. Wear 2016; 66-367: 188-93.

[12] Ignesti M, Malvezzi M, Marini L, et al. Development of a wear model for the prediction of wheel and rail profile evolution in railway systems. Wear 2012; 284-285: 1-17.

[13] Innocenti A, Marini L, Meli E, et al. Development of a wear model for the analysis of complex railway networks. Wear 2014; 309: 174-91.

[14] Nejad RM, Shariati M, Farhangdoost K. Effect of wear on rolling contact fatigue crack growth in rails. Tribol Int 2016; 94: 118-25.

[15] Taraf M, Zahaf EH, Oussouaddi O, et al. Numerical analysis for predicting the rolling contact fatigue crack initiation in a railway wheel steel. Tribol Int 2010; 43:585-93.

[16] Stefano C, Steven C. The competitive role of wear and RCF: Full scale experimental assessment of artificial and natural defects in railway wheel treads. Wear 2016; 366-367: 325-37.

[17] Gao N, Dwyer-Joyce RS. The effects of surface defects on the fatigue of water-and oil-lubricated contacts. Proc Instn Mech Engrs: Part J 2000; 214: 611-26.

[18] Gao N, Dwyer-Joyce RS, Grieve DG. Disc machine testing to assess the life of surface-damaged railway track. Proc Instn Mech Engrs: Part F 2001; 215: 261-75.

[19] Seo JW, Kwon SK, Lee DH. Effects of surface defects on rolling contact fatigue of rail. Procedia Engineering 2011; 10: 274-78.

[20] Zhao XJ, Guo J, Wang HY, et al, Effects of decarburization on the wear resistance and damage mechanisms of rail steels subject to contact fatigue. Wear 2016; 364-365: 130-43.

[21] UIC standard, 712R, rail defect, 4th edition. 2002

[22] Li G, Hong ZY, Yan QZ. The influence of microstructure on the rolling contact fatigue of steel for high-speed-train wheel Wear. 2015; 342-343: 349-55.

[23] Dylewskia B, Risbetb M, Bouvierb S et al. The tridimensional gradient of microstructure in worn rails-Experimental characterization of plastic deformation accumulated by RCF. Wear 2017; 392-393: 50-9.

[24] Olofsson U, Zhu Y, S Abbasi. Tribology of the wheel–rail contact – aspects of wear,

particle emission and adhesion. Vehicle System Dynamics. 2013; 51: 1091-120.

[25] Fletcher DI, Lewis SR. Creep curve measurement to support wear and adhesion modelling, using a continuously variable creep twin disc machine. Wear. 2013; 298 299: 57-65.

[26] Pearson S. Initiation of fatigue cracks in commercial aluminium alloys and the subsequent propagation of very short cracks. Eng Frac. Mech 1975; 7: 241-47.

[27] Eden HC, Garnham JE, Davis CL. Influential microstructural changes on rolling contact fatigue crack initiation in pearlitic rail steels. Mater. Sci. Technol 2005; 21: 623-29.

[28] Garnham JE, Davis CL. Very early stage rolling contact fatigue crack growth in pearlitic rail steels. Wear 2011; 271: 100-12,

Figure caption

Fig.1: Schematic diagram of the machine.

Fig.2 Scheme size of the wheel and rail rollers.

Fig.3: Scheme of dents on wheel/rail simple before testing, (a) rail; (b) wheel.

Fig.4: SEM micrographs of surface damage of rail rollers, (a) RN; (b) RS; (c) RM; (d) RL.

Fig.5: SEM micrographs of surface damage of wheel rollers, (a) WN; (b) WS; (c) WM; (d) WL.

Fig.6: OM micrographs of plastic deformation of rail rollers, (a) RS; (b) RM; (c) RL.

Fig.7: OM micrographs of plastic deformation of wheel rollers, (a) WS; (b) WM; (c) WL.

Fig.8: OM micrographs of fatigue cracks on the section of rail rollers, (a) RN; (b) RS; (c) RM; (d) RL.

Fig.9: SEM micrographs of fatigue cracks on the section of rail rollers, (a) RN; (b) RS; (c) RM; (d) RL

Fig.10: SEM micrographs of fatigue cracks on the section of wheel rollers, (a) WN; (b) WS; (c) WM; (d) WL

Fig.11: EBSD micrographs of grain boundary on wheel/rail rollers, (a) WN; (b) WM (in the front of dent); (c) WM (in the rear of dent); (d) RM (in the front of dent); (e) RM (in the rear of dent)

Fig.12: Inverse pole figure (IPF) of wheel/rail rollers, (a) WN; (b) WM (in the front of dent); (c) WM (in the rear of dent); (d) RM (in the front of dent); (e) RM (in the rear of dent)

Fig.13: Strain contouring of wheel/rail rollers, (a) WN; (b) WM (in the front of dent); (c) WM (in the rear of dent); (d) RM (in the front of dent); (e) RM (in the rear of dent)

Fig.14: Crack growth mechanism around the rail dent, (a) in early cycles; (b) in final cycles.

Fig.15: Crack growth mechanism around the wheel dent, (a) early cycles; (b) the next cycles (direction of tangential force changed).

Fig.1

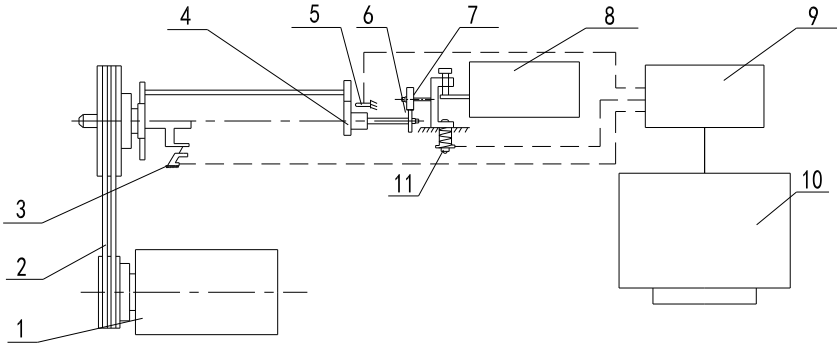

1. DC motor; 2. Drive belt; 3. Torque sensor; 4. Drive shaft gears; 5. Photosensor; 6. Lower roller; 7. Upper roller; 8. Driven shaft gears; 9. Controller; 10. Computer; 11. Load sensor

Fig. 2

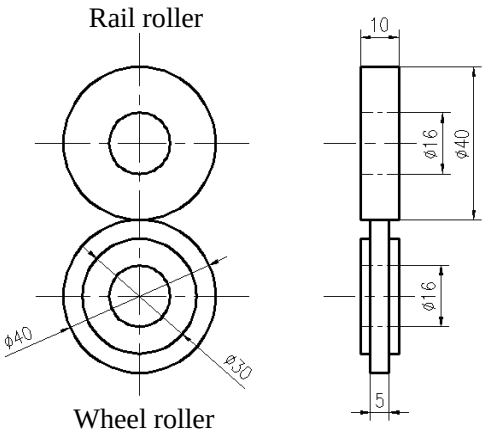

Fig.3

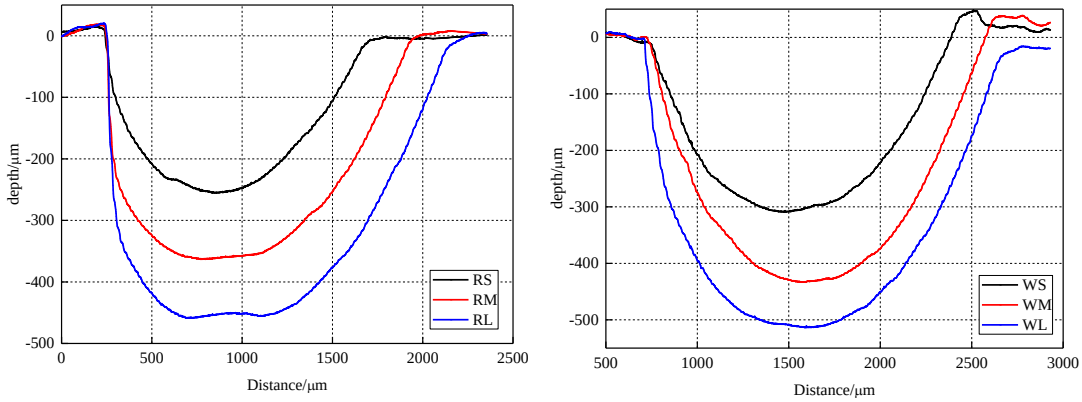
0
-100
-200
-300
-400
-500
depth/μm
0
500
1000
1500
2000
2500
Distance/μm
RS
RM
RL
0
-100
-200
-300
-400
-500
depth/μm
500
1000
1500
2000
2500
3000
Distance/μm
WS
WM
WL

(a) (b)

Fig.4

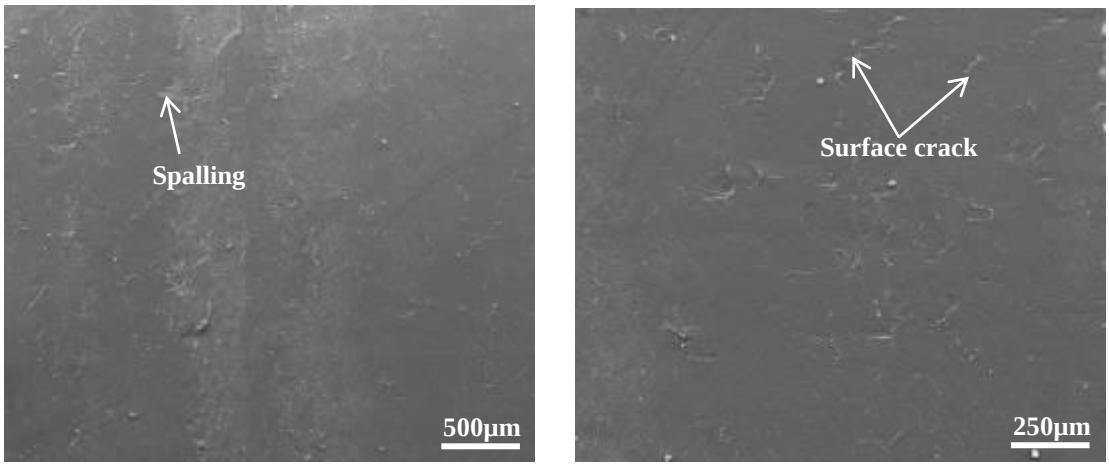
Spalling
500μm
Surface crack
250μm

(a)

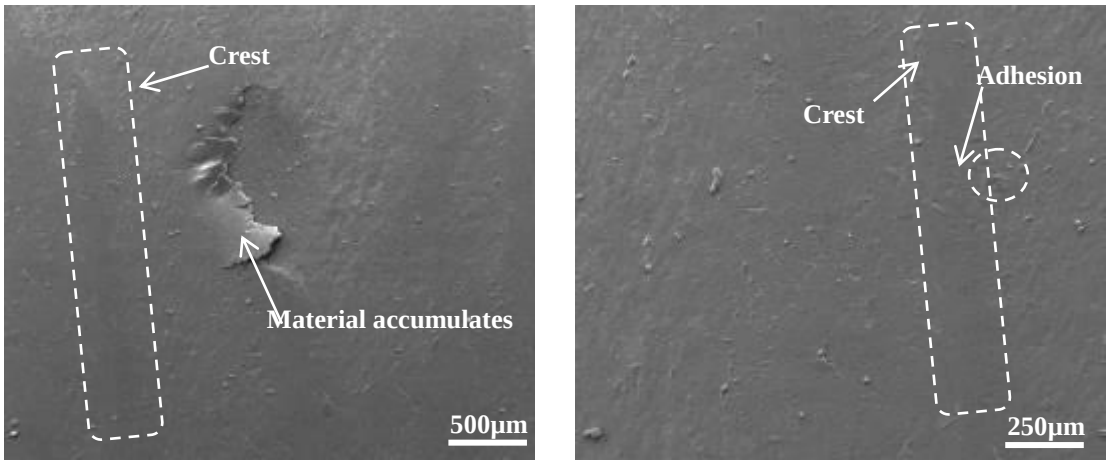
Crest
Material accumulates
500μm
Crest
Adhesion
250μm

(b)

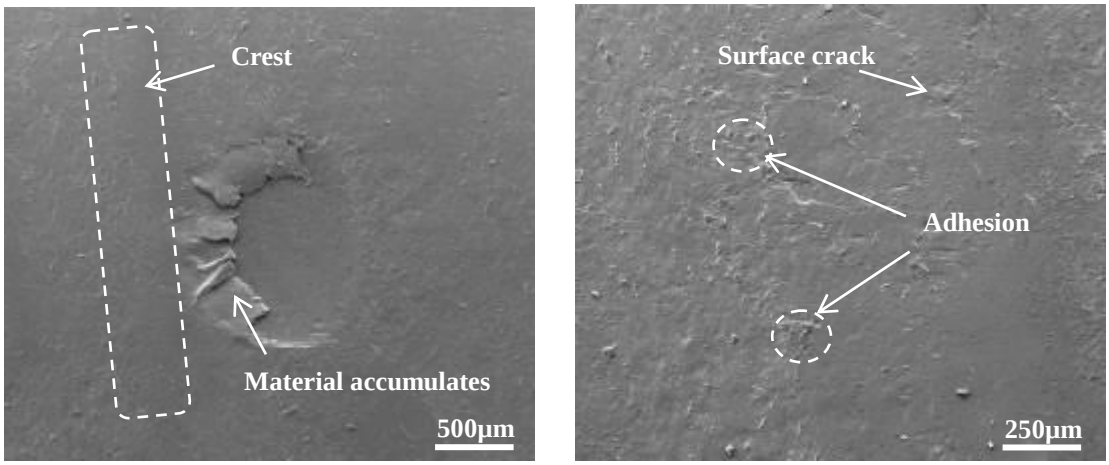
Crest
Material accumulates
500μm
Surface crack
Adhesion
250μm

(c)

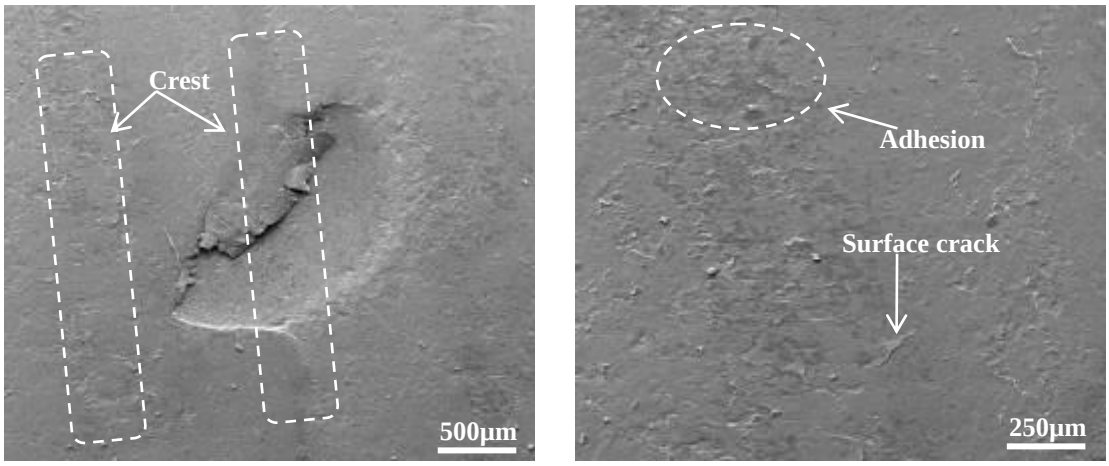

(d)

Fig.5

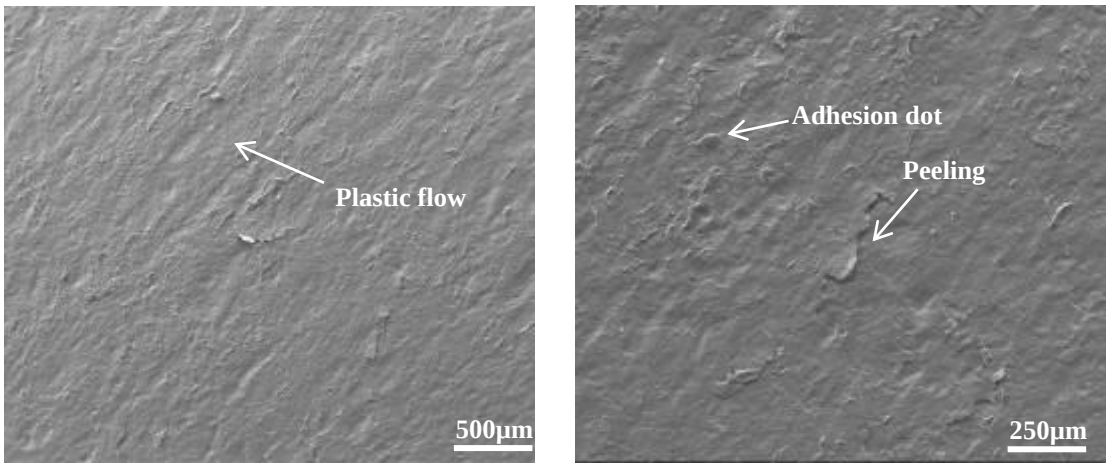
Plastic flow
500μm
Adhesion dot
Peeling
250μm

(a)

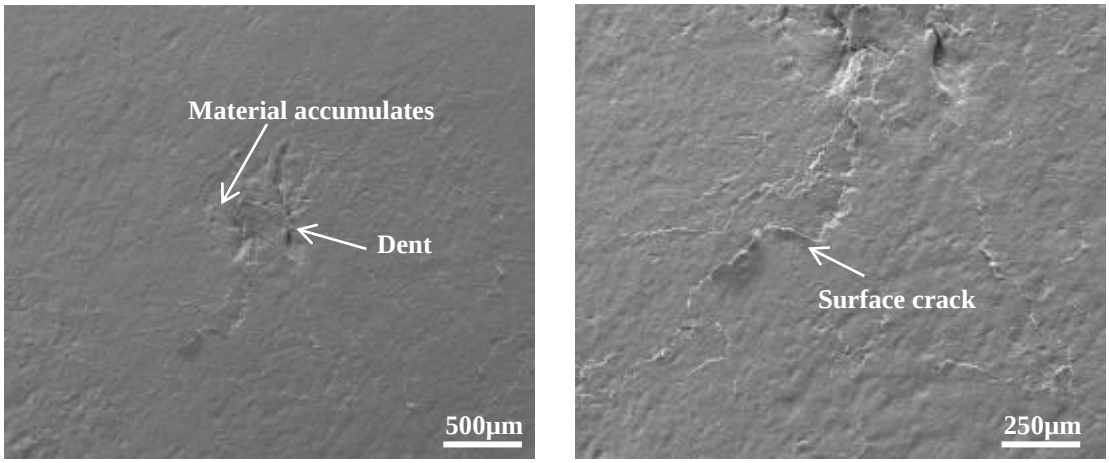
Material accumulates
Dent
500μm
Surface crack
250μm

(b)

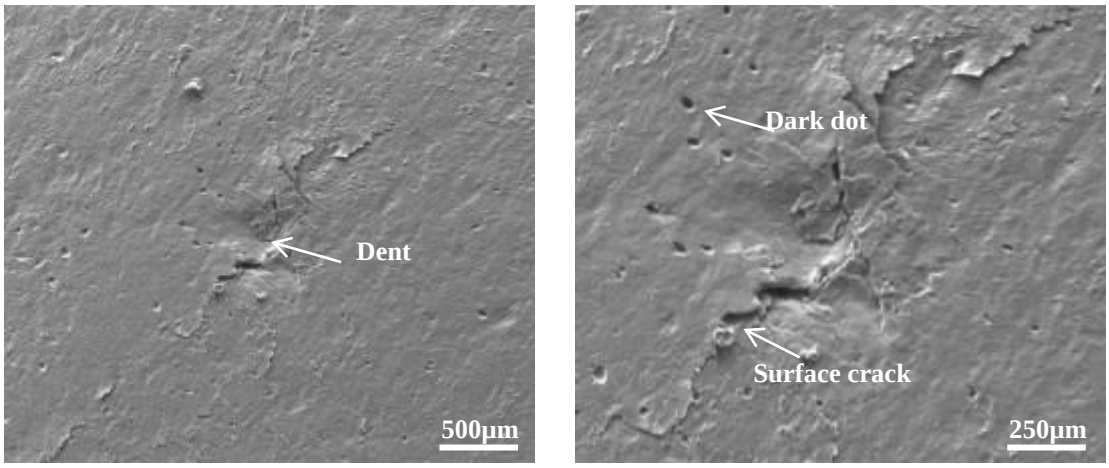
Dent
500μm
Dark dot
Surface crack
250μm

(c)

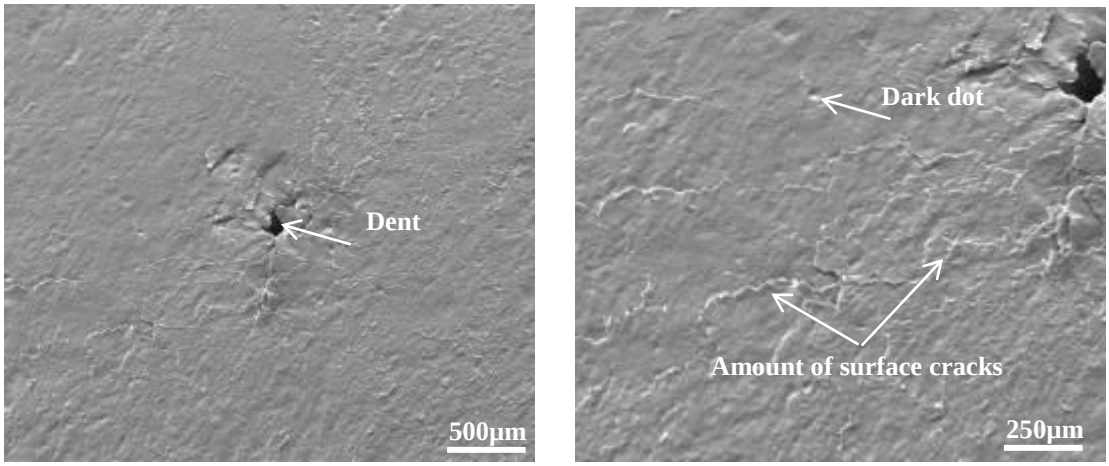

(d)

Fig.6

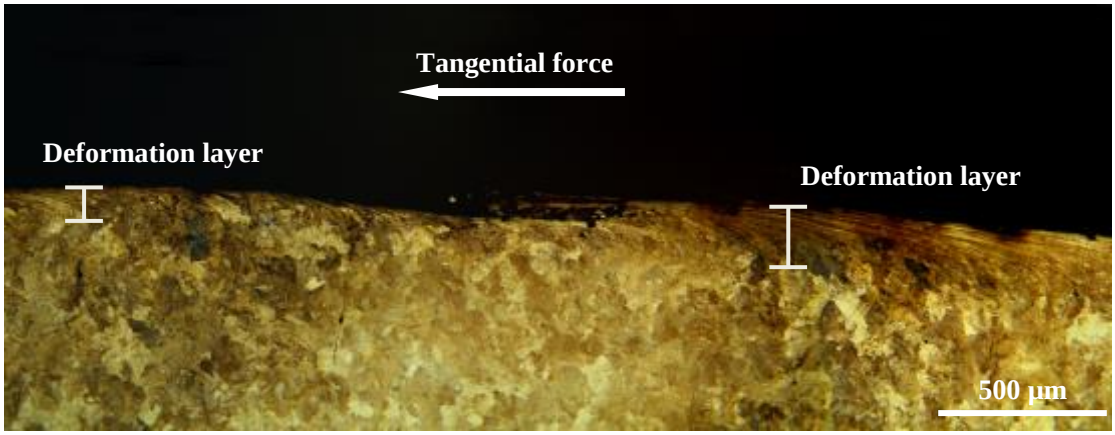
Tangential force
Deformation layer
Deformation layer
500 μm

(a)

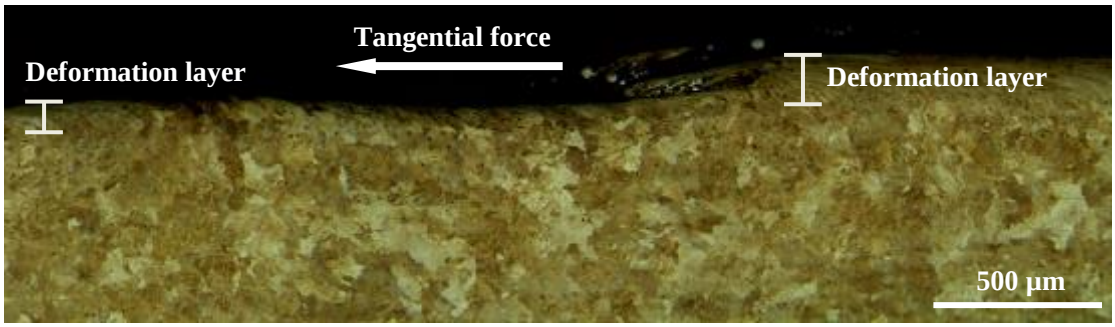
Tangential force
Deformation layer
Deformation layer
500 μm

(b)

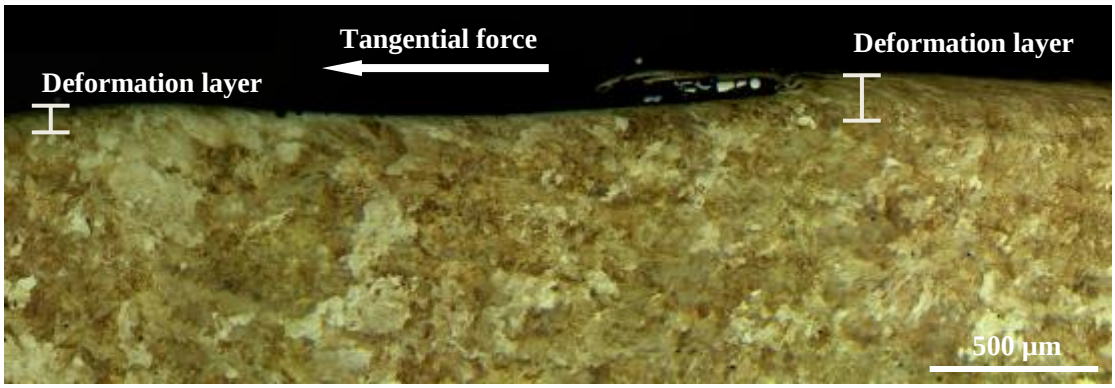
Tangential force
Deformation layer
Deformation layer
500 μm

(c)

Fig.7

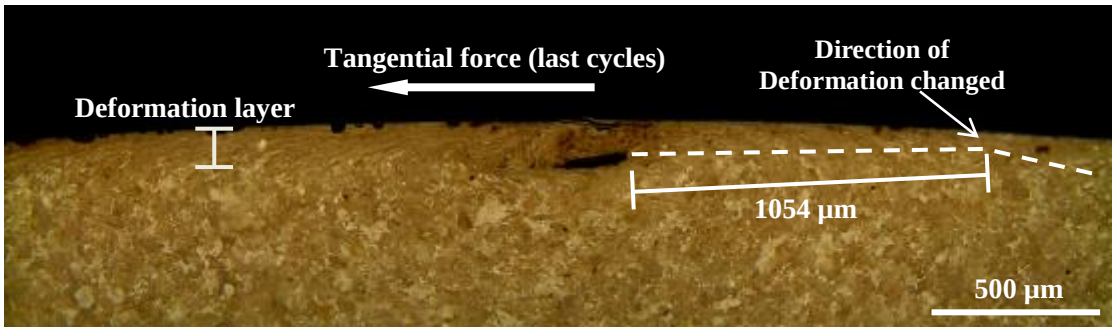
Tangential force (last cycles)
Direction of
Deformation changed
Deformation layer
1054 µm
500 µm

(a)

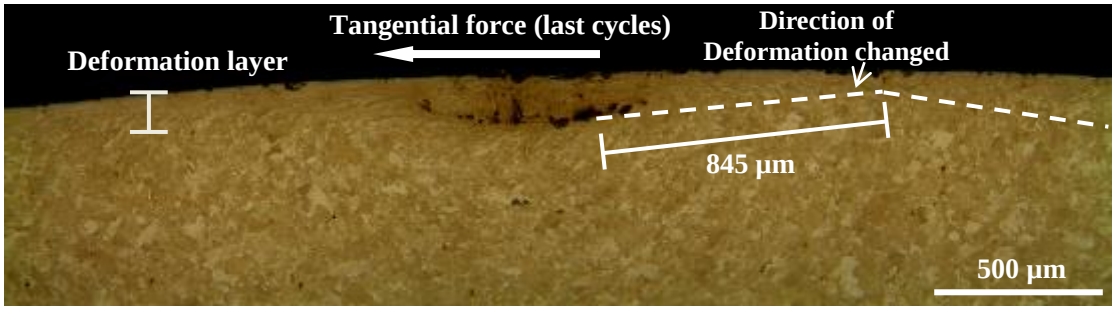
Tangential force (last cycles)
Direction of
Deformation changed
Deformation layer
845 µm
500 µm

(b)

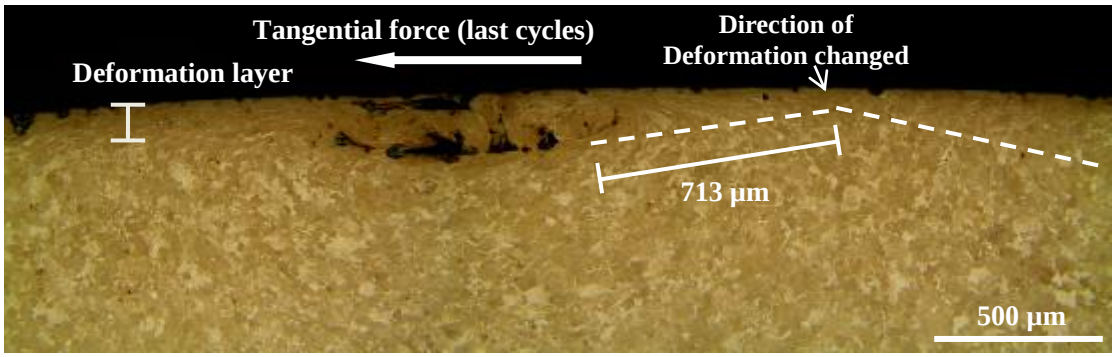
Tangential force (last cycles)
Direction of
Deformation changed
Deformation layer
713 µm
500 µm

(c)

Fig.8

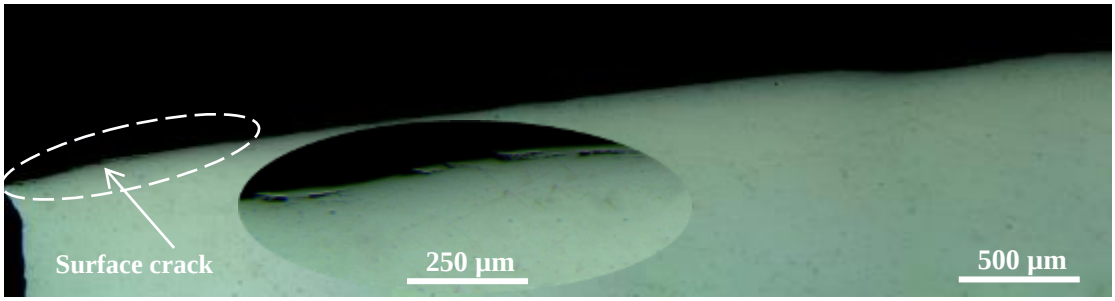
Surface crack
250 µm
500 µm

(a)

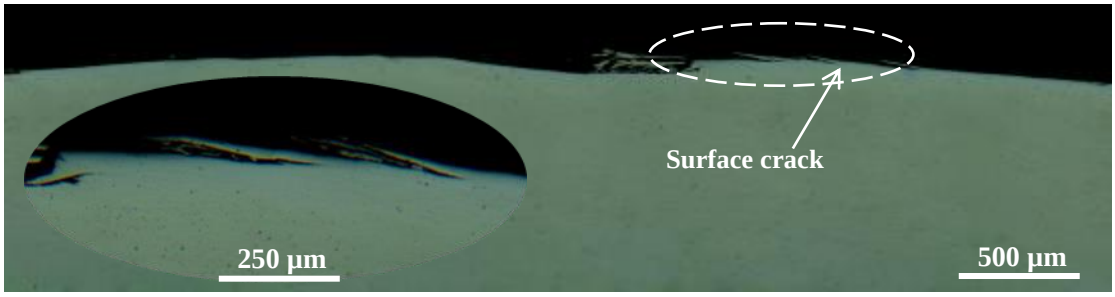
Surface crack
250 µm
500 µm

(b)

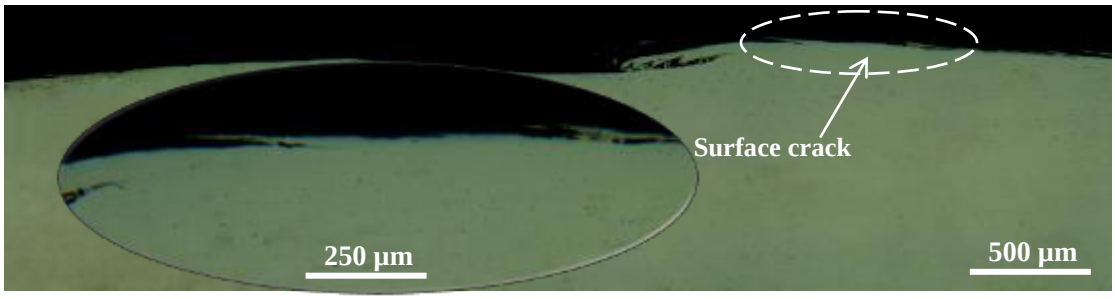
Surface crack
250 µm
500 µm

(c)

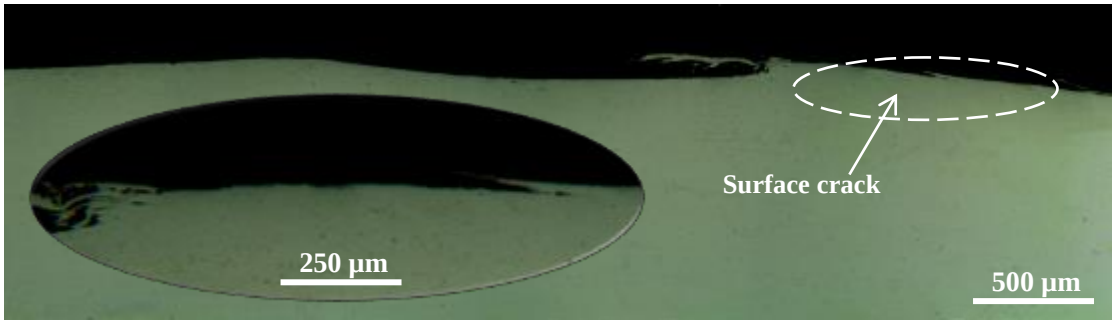
Surface crack
250 µm
500 µm

(d)

Fig.9

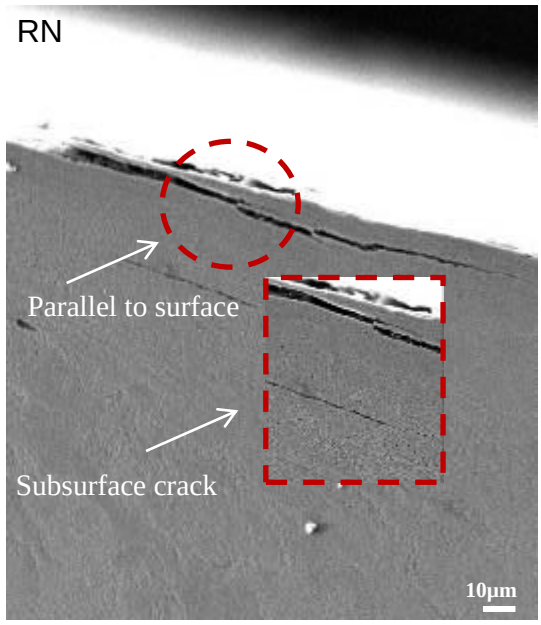
RN
Parallel to surface
Subsurface crack
10μm

(a)

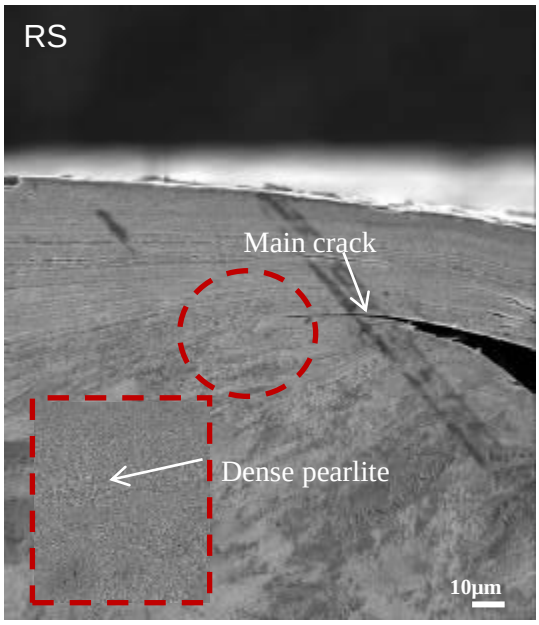
RS
Main crack
Dense pearlite
10μm

(b)

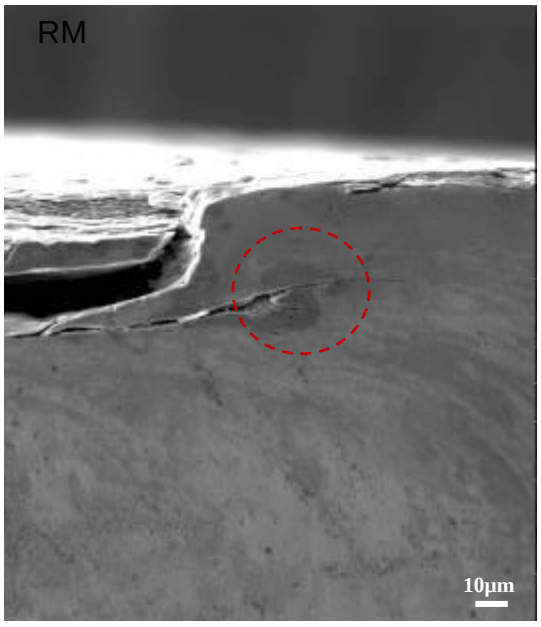
RM
10μm

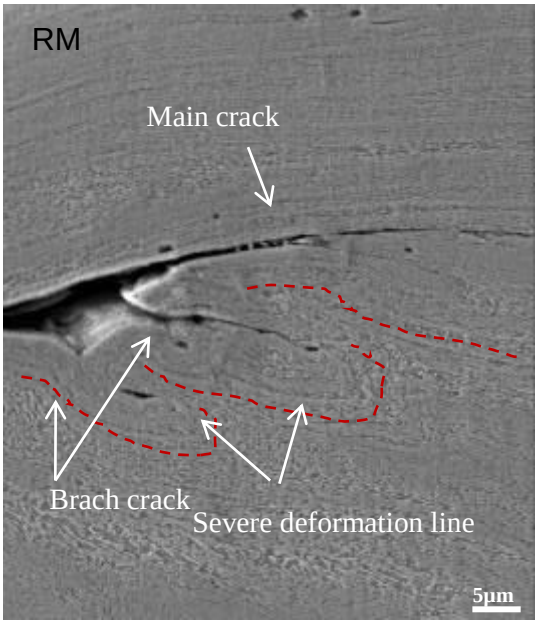
RM
Main crack
Brach crack
Severe deformation line
5μm

(c)

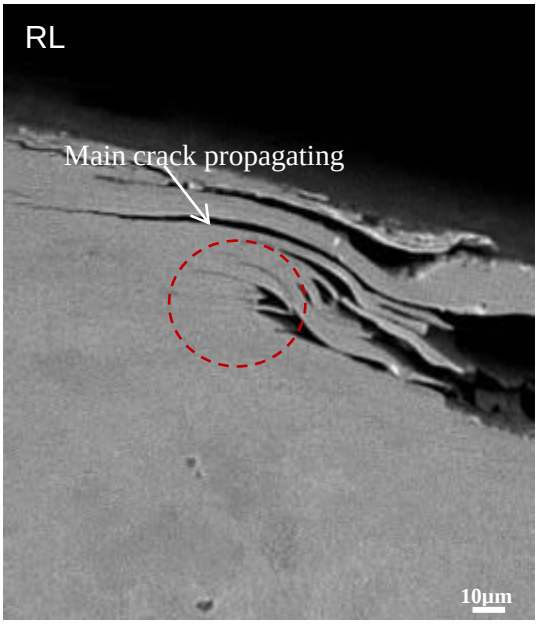
RL
Main crack propagating
10μm

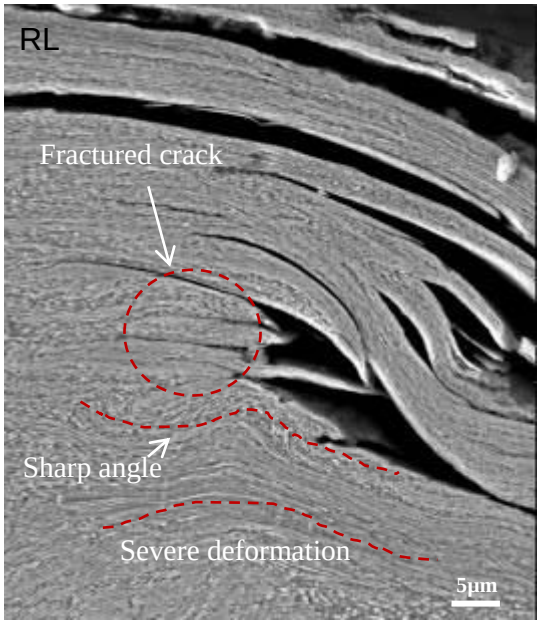
RL
Fractured crack
Sharp angle
Severe deformation
5μm

(d)

Fig.10

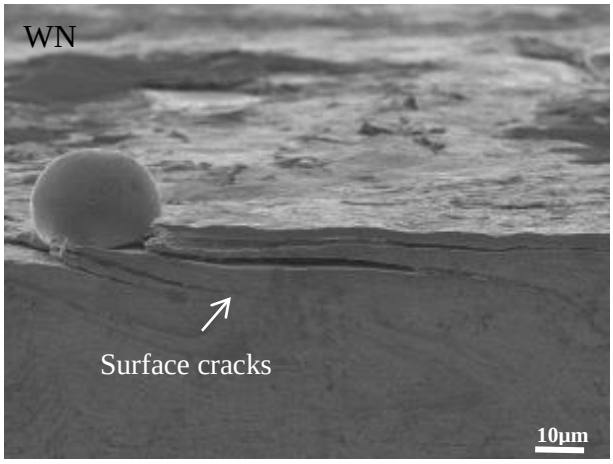
WN
Surface cracks
10μm

(a)

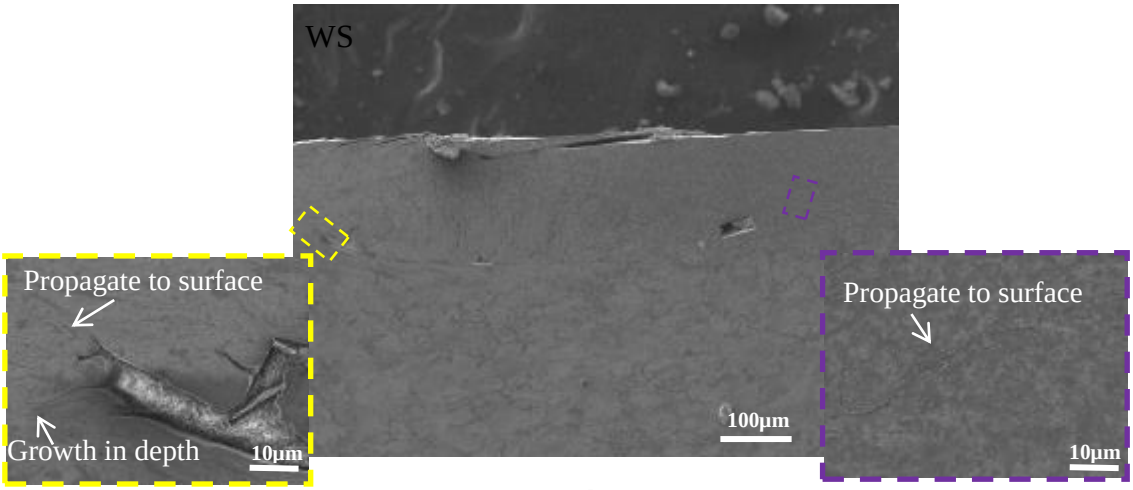
WS
Propagate to surface
Growth in depth
10μm
100μm
Propagate to surface
10μm

(b)

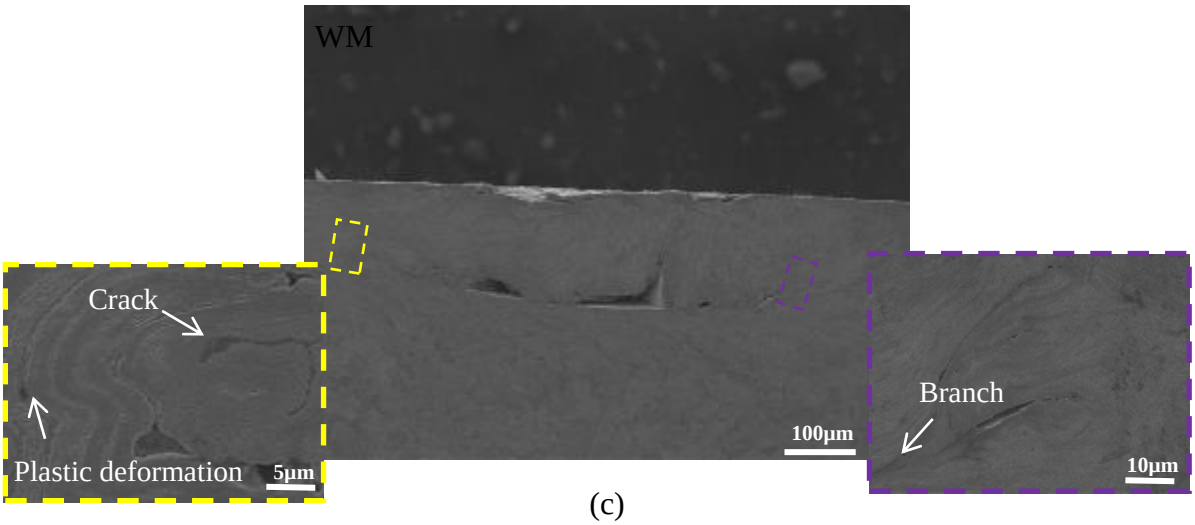
WM
Crack
Plastic deformation
5μm
100μm
Branch
10μm

(c)

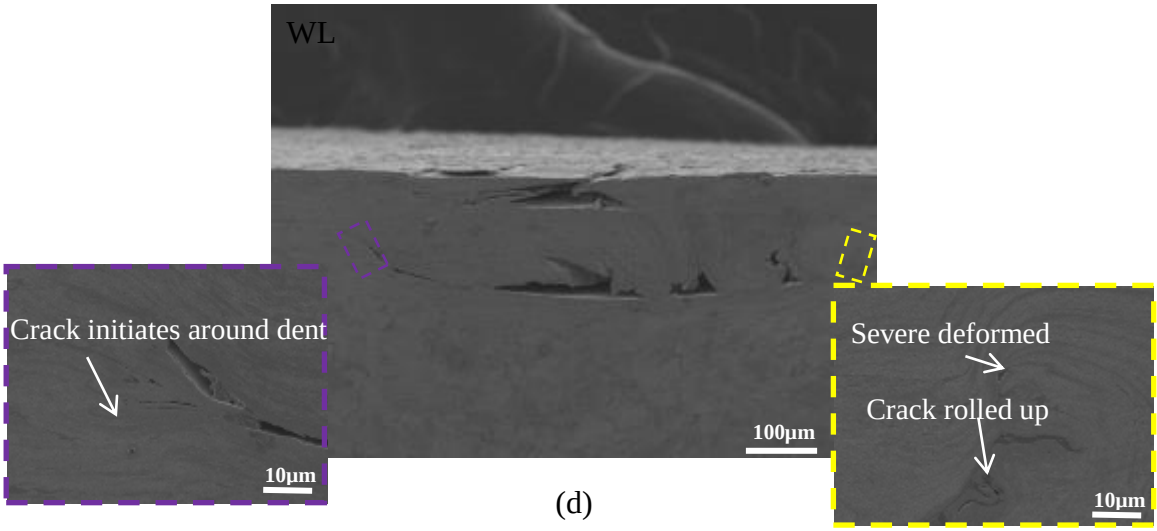
WL
Crack initiates around dent
10μm
100μm
Severe deformed
Crack rolled up
10μm

(d)

Fig.11

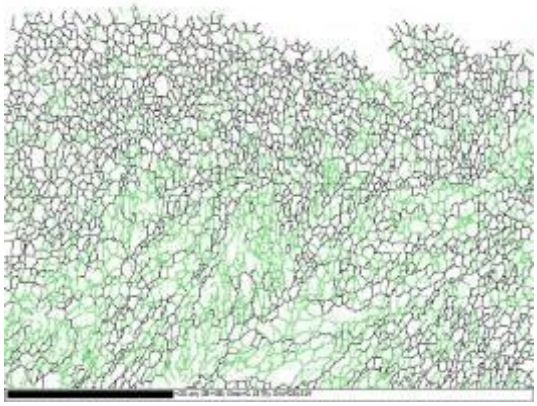

(a)

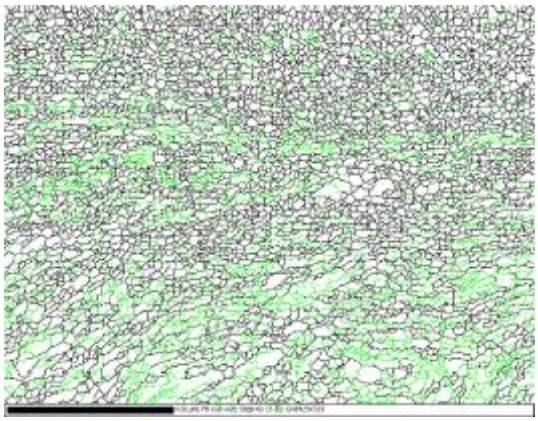

(b)

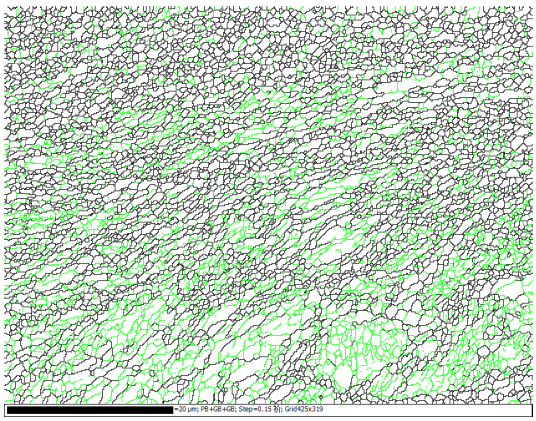

(c)

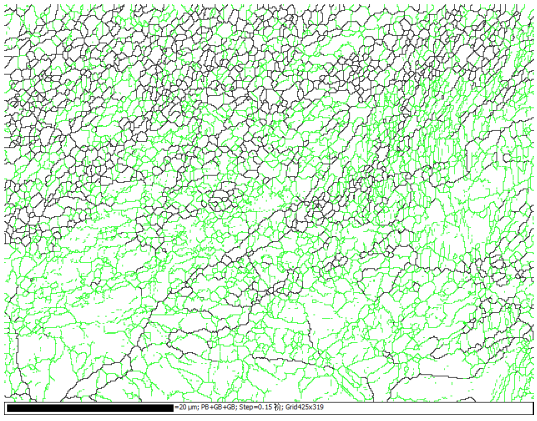

(d)

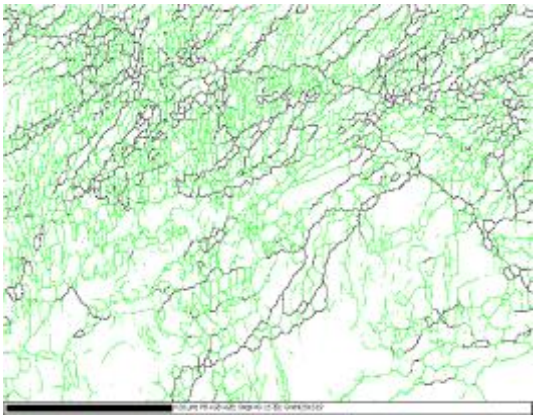

(e)

Fig.12

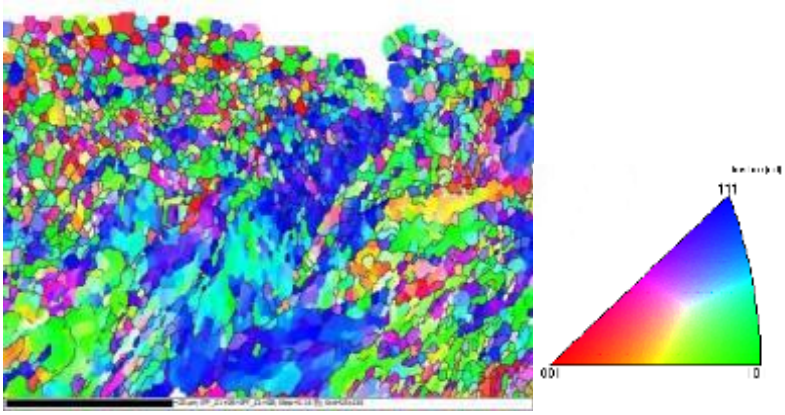

(a)

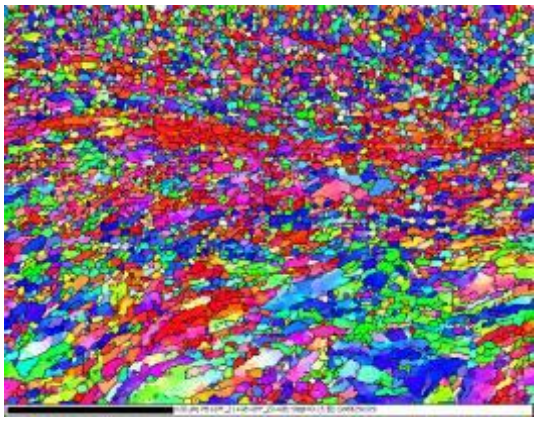

(b)

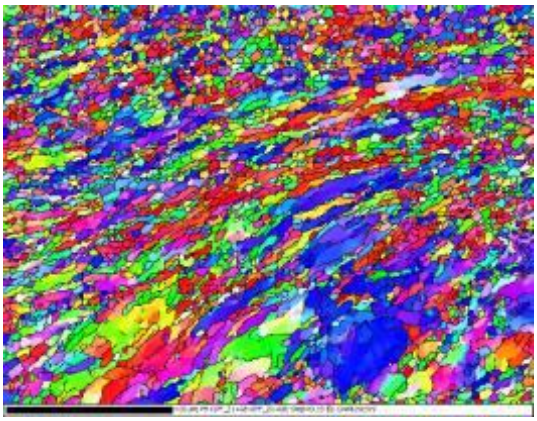

(c)

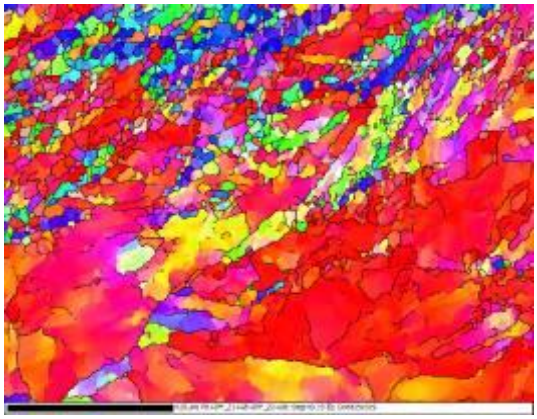

(d)

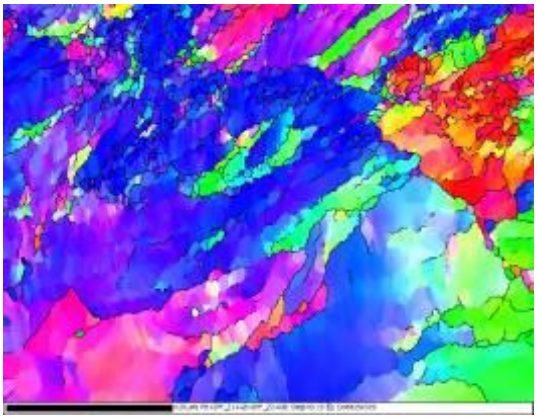

(e)

Fig.13

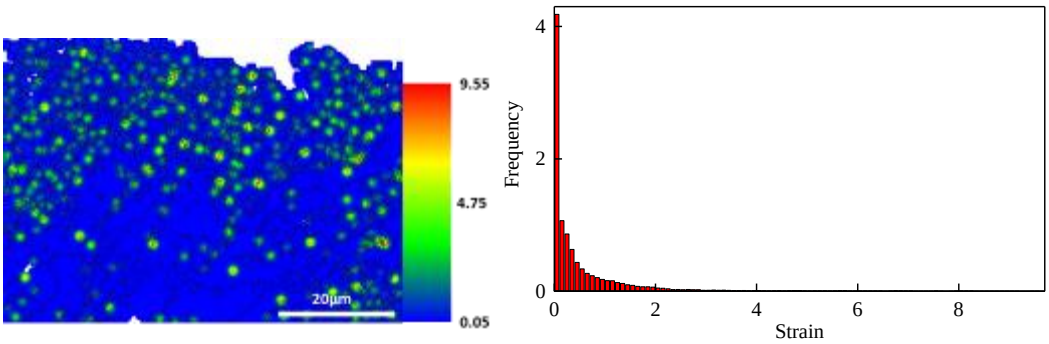
9.55
4.75
0.05
20μm
Frequency
Strain
0
2
4
6
8

(a)

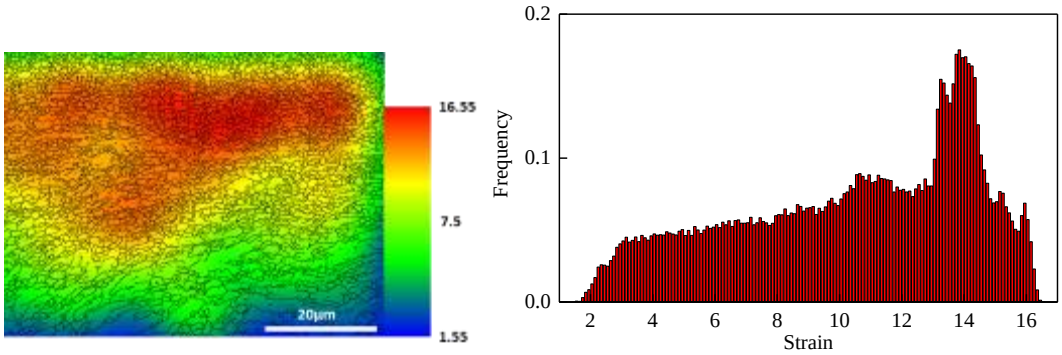
16.55
7.5
1.55
20μm
Frequency
Strain
0.0
0.1
0.2
2
4
6
8
10
12
14
16

(b)

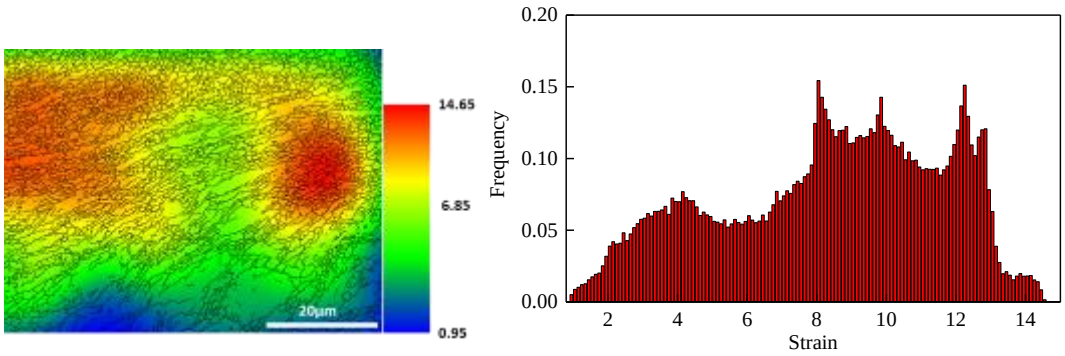
14.65
6.85
0.95
20μm
Frequency
Strain
0.00
0.05
0.10
0.15
0.20
2
4
6
8
10
12
14

(c)

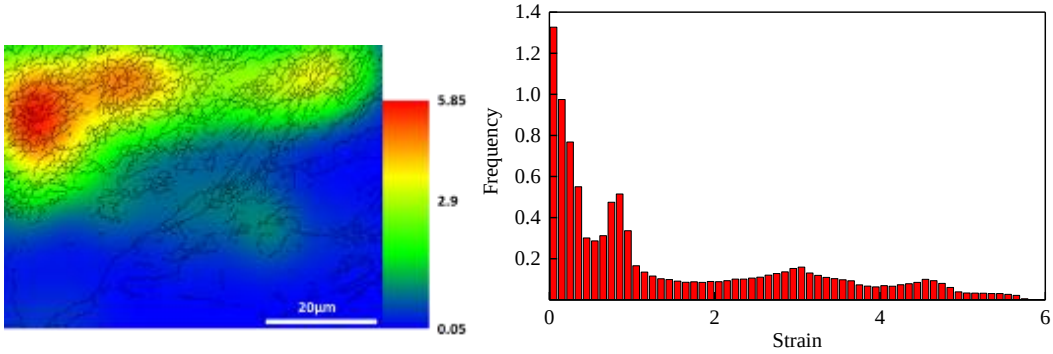
5.85
2.9
0.05
20μm
Frequency
1.4
1.2
1.0
0.8
0.6
0.4
0.2
0
2
4
6
Strain

(d)

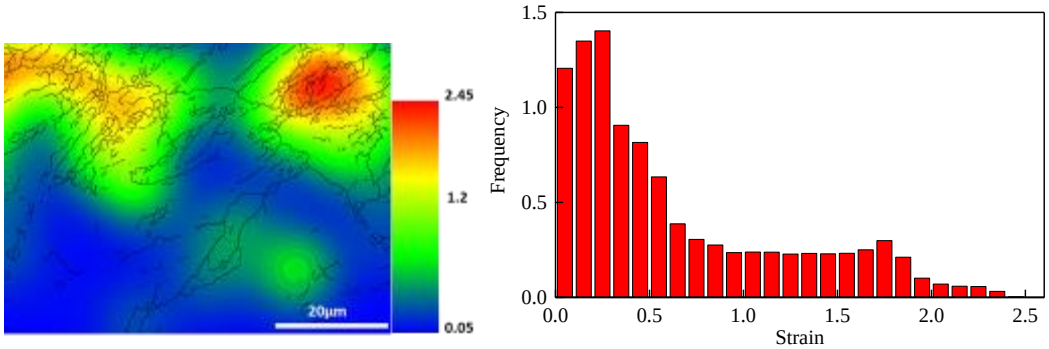
2.45
1.2
0.05
20μm
Frequency
1.5
1.0
0.5
0.0
0.0
0.5
1.0
1.5
2.0
2.5
Strain

(e)

Fig.14

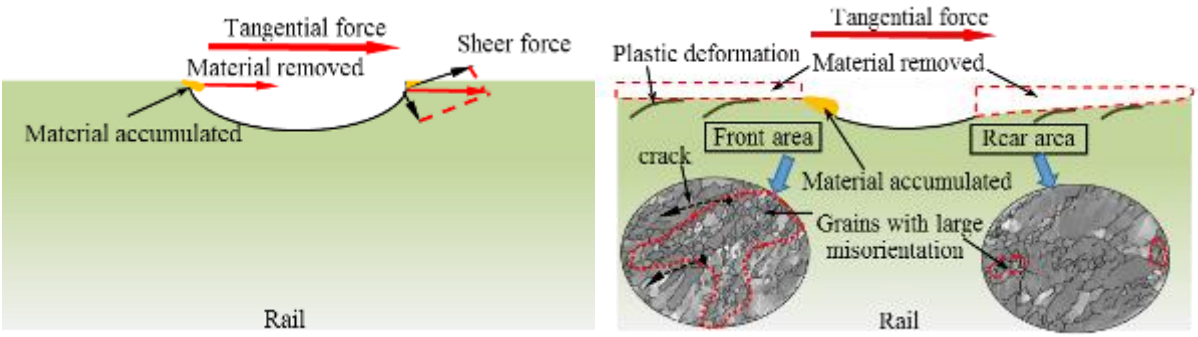
Tangential force
Material removed
Sheer force
Material accumulated
Rail
Tangential force
Plastic deformation
Material removed
Front area
Rear area
crack
Material accumulated
Grains with large misorientation
Rail

(a) (b)

Fig. 15

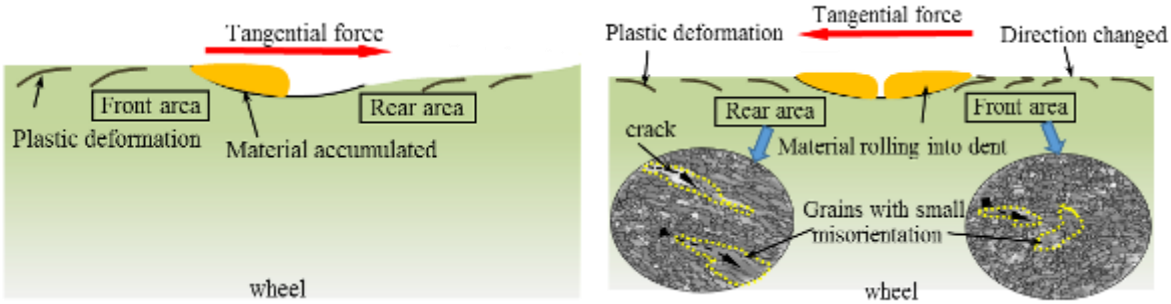
Tangential force
Front area
Rear area
Plastic deformation
Material accumulated
wheel
Plastic deformation
Tangential force
Direction changed
Rear area
Front area
crack
Material rolling into dent
Grains with small misorientation
wheel

(a) (b)

Table caption

Table 1: Chemical compositions of wheel and rail rollers (wt %).

Table 2: Experimental details.

Table 3: Statistic of surface cracks on rail rollers.

Table 4: Crack propagating types on wheel/rail rollers.

Table 1

Roller	C	Si	Mn	P	S
Wheel	0.56~0.60	≤0.40	≤0.80	≤0.020	≤0.015
Rail	0.65~0.75	0.10~0.50	0.80~1.30	≤0.025	≤0.025

Table 2

Test roller	Size of dents	Rolling direction	Matched roller
RS	Rail roller with small dents	Unchanged	WN
RM	Rail roller with middle dents	Unchanged	WN
RL	Rail roller with large dents	Unchanged	WN
RN	Rail roller without dent	Unchanged	WN
WS	Wheel roller with small dents	Changed per 12000 cycles	RN
WM	Wheel roller with middle dents	Changed per 12000 cycles	RN
WL	Wheel roller with large dents	Changed per 12000 cycles	RN
WN	Wheel roller without dent	Changed per 12000 cycles	RN

Table 3

	Length of crack/μm		Angle of crack/°	
	Rear of defect	Front of defect	Rear of defect	Front of defect
RS	202.67±5.13	180±4.08	8.75±2.22	7.75±2.22
RM	215.28±10.5	157.35±6.99	9.25±2.22	5±0.82
RL	250±10.61	142.22±11.85	10.33±1.53	7±2.55
RN	120±11.93		6.75±1.71	

Table 4

	Branch	Subsurface crack	Small angle(<10°)	Growth to surface	Growth to depth
RS		×	×		
RM	×		×		×
RL		×	×	×	
RN		×	×	×	
WS	×		×	×	×
WM	×		×	×	×
WL	×		×	×	×
WN			×	×	